Title

Acute reversal of phospholamban inhibition facilitates the rhythmic whole-cell propagating calcium waves in isolated ventricular myocytes.

Authors

Chan, Yi-Hsin
Tsai, Wei-Chung
Song, Zhen
et al.

Publication Date

2015-03-01

DOI

10.1016/j.yjmcc.2014.12.024

Peer reviewed

Journal of Molecular and Cellular Cardiology 80 (2015) 126–135

Contents lists available at ScienceDirect

Journal of Molecular and Cellular Cardiology

journal homepage: www.elsevier.com/locate/yjmcc

Original article

Acute reversal of phospholamban inhibition facilitates the rhythmic whole-cell propagating calcium waves in isolated ventricular myocytes

Yi-Hsin Chan [a,b], Wei-Chung Tsai [a,c], Zhen Song [d], Christopher Y. Ko [d], Zhilin Qu [d], James N. Weiss [d], Shien-Fong Lin [a,e], Peng-Sheng Chen [a], Larry R. Jones [a], Zhenhui Chen [a,*]

[a] Krannert Institute of Cardiology and Division of Cardiology, Department of Medicine, Indiana University School of Medicine, Indianapolis, IN, USA
[b] Division of Cardiology, Department of Internal Medicine, Chang Gung Memorial Hospital, Chang Gung University College of Medicine, Linkou, Taoyuan, Taiwan
[c] Division of Cardiology, Department of Internal Medicine, Kaohsiung Medical University Hospital, Kaohsiung University College of Medicine, Kaohsiung, Taiwan
[d] Division of Cardiology, Department of Medicine, University of California, Los Angeles, CA, USA
[e] Institute of Biomedical Engineering, National Chiao-Tung University, Hsin-Chu, Taiwan

ARTICLE INFO

Article history:
Received 23 September 2014
Received in revised form 8 December 2014
Accepted 30 December 2014
Available online 14 January 2015

Keywords:
Calcium
Sarcoplasmic reticulum
Phospholamban
Spontaneous calcium waves

ABSTRACT

Phospholamban (PLB) inhibits the activity of cardiac sarcoplasmic reticulum (SR) Ca^{2+}-ATPase (SERCA2a). Phosphorylation of PLB during sympathetic activation reverses SERCA2a inhibition, increasing SR Ca^{2+} uptake. However, sympathetic activation also modulates multiple other intracellular targets in ventricular myocytes (VMs), making it impossible to determine the specific effects of the reversal of PLB inhibition on the spontaneous SR Ca^{2+} release. Therefore, it remains unclear how PLB regulates rhythmic activity in VMs.

Here, we used the Fab fragment of 2D12, a monoclonal anti-PLB antibody, to test how acute reversal of PLB inhibition affects the spontaneous SR Ca^{2+} release in normal VMs. Ca^{2+} sparks and spontaneous Ca^{2+} waves (SCWs) were recorded in the line-scan mode of confocal microscopy using the Ca^{2+} fluorescent dye Fluo-4 in isolated permeabilized mouse VMs. Fab, which reverses PLB inhibition, significantly increased the frequency, amplitude, and spatial/temporal spread of Ca^{2+} sparks in VMs exposed to 50 nM free [Ca^{2+}]. At physiological diastolic free [Ca^{2+}] (100–200 nM), Fab facilitated the formation of whole-cell propagating SCWs. At higher free [Ca^{2+}], Fab increased the frequency and velocity, but decreased the decay time of the SCWs. cAMP had little additional effect on the frequency or morphology of Ca^{2+} sparks or SCWs after Fab addition. These findings were complemented by computer simulations. In conclusion, acute reversal of PLB inhibition alone significantly increased the spontaneous SR Ca^{2+} release, leading to the facilitation and organization of whole-cell propagating SCWs in normal VMs. PLB thus plays a key role in subcellular Ca^{2+} dynamics and rhythmic activity of VMs.

1. Introduction

The rate at which Ca^{2+} is pumped into the lumen of cardiac sarcoplasmic reticulum (SR) by the SR Ca^{2+}-ATPase (SERCA2a) is tightly controlled by the regulatory protein phospholamban (PLB) [1,2]. Dephosphorylated PLB inhibits SERCA2a activity while increased β-adrenergic stimulation phosphorylates PLB by cAMP–dependent protein kinase A (PKA) and Ca^{2+}/calmodulin-dependent protein kinase (CaMKII), reversing SERCA2a inhibition, thus enhancing the Ca^{2+} uptake into cardiac SR [3,4]. Multiple studies in living ventricular myocytes (VMs) treated with isoproterenol or the monoclonal anti-PLB antibody 2D12 [5,6], or isolated from PLB transgenic and knockout (PLB-KO) mice [7–10] have demonstrated that PLB modulates intracellular Ca^{2+} dynamics, regulating both inotropy and lusitropy.

In diastole, SR Ca^{2+} may be released via cardiac ryanodine receptor channel (RyR2) as Ca^{2+} sparks or spontaneous Ca^{2+} waves (SCWs), a process that is important to physiological rhythm and pathophysiological conditions such as the formation of delayed afterdepolarizations (DADs) and the syndrome of catecholaminergic polymorphic ventricular tachycardia (CPVT) [11–13]. The regulation of spontaneous SR Ca^{2+} release is very complicated, and involves many regulatory factors including both cytoplasmic and lumenal Ca^{2+} [14], multiple protein kinases (e.g., PKA and CaMKII) [15–17], and junctional regulatory protein complexes [18,19]. Within this complex system, the specific role of PLB in the regulation of spontaneous SR Ca^{2+} release during β-adrenergic stimulation in VMs remains unclear. One reason is that besides PLB, β-adrenergic stimulation also phosphorylates RyR2 and other Ca^{2+} handling proteins regulating the SR Ca^{2+} release, making it impossible to

Abbreviations: 2D12, anti-PLB monoclonal antibody; CaMKII, Ca^{2+}/calmodulin-dependent protein kinase; CPVT, catecholaminergic polymorphic ventricular tachycardia; DAD, delay afterdepolarizations; Fab, fab fragment of 2D12; K_{Ca}, Ca concentration for half-maximal effect; PKA, cAMP-dependent protein kinase A; PLB, phospholamban; PLB-KO, PLB deficiency mice; RyR2, cardiac ryanodine receptor channel; SCW, spontaneous calcium wave; SERCA2a, isoform of sarco(endo)plasmic reticulum Ca^{2+}-ATPase in cardiac sarcoplasmic reticulum; SR, sarcoplasmic reticulum; VM, ventricular myocytes.

* Corresponding author at: Krannert Institute of Cardiology, 1800 N. Capitol Ave., Indianapolis, IN, 46202, USA. Tel.: +1 317 274 0964; fax: +1 317 962 0505.
E-mail address: zhechen@iu.edu (Z. Chen).

http://dx.doi.org/10.1016/j.yjmcc.2014.12.024
0022-2828/

delineate whether the reversal of PLB inhibition alone is sufficient to augment spontaneous SR Ca^{2+} release and cause cell-wide SCWs. Previous studies using PLB-KO mice suggest that PLB ablation increases inotropy but not chronotropy [7]. However, the chronic absence of PLB induces multiple adaptive changes of intracellular Ca^{2+} handling proteins [20,21]. The specific role of PLB in rhythmic control in VM remains unclear.

PLB, as a key component of the Ca^{2+} clock, has also been shown to influence rhythmic activity of sinoatrial node cells [22]. Recent studies also indicate that PLB plays a key role in modulating the rhythmic Ca^{2+} activity in VMs. In particular, Kapoor *et al.* demonstrated that expression of Tbx18 induced rhythmic intracellular Ca^{2+} cycling events in VMs, mimicking the "Ca^{2+} clock" of native sinoatrial node cells. In this process, phosphorylation of PLB was 65-fold higher than that in the control VMs, indicating that the modulation of PLB helps to generate rhythmic activity [23]. Sirenko *et al.* also demonstrated that permeabilized VMs showed increased spontaneous Ca^{2+} releases with the self-organized and partial synchronization of Ca^{2+} sparks after PLB inhibition by drugs or 2D12 [24]. On the other hand, Bai *et al.* demonstrated that despite severe SR Ca^{2+} leak with multiple Ca^{2+} sparks or small wavelets, VMs from PLB-KO mice break up the formation of organized and whole-cell propagating SCWs in triggering the DADs [25]. They further showed that PLB ablation actually suppressed triggered activity and stress-induced ventricular tachycardia in the mouse model of PLB-KO plus RyR2 mutation. While these studies point to the regulation of rhythmic Ca^{2+} activity by PLB in VM, an important question that remains to be addressed is whether accelerating SR Ca^{2+} uptake by specifically removing PLB inhibition of the Ca^{2+} pump is pro-arrhythmic (i.e. increasing the automaticity in normal VMs) [24] or anti-arrhythmic (i.e. suppressing the DADs in the CPVT model) [25] in the VMs.

In this study, we took advantage of the specific action of the Fab fragment of the monoclonal anti-PLB antibody 2D12 in blocking the interaction between PLB and SERCA2a in isolated permeabilized (skinned) murine VMs [5,6,26]. We demonstrate that acute and specific reversal of PLB inhibition can significantly increase the frequency, amplitude, and spatial/temporal spread of Ca^{2+} sparks, leading to the facilitation and organization of whole-cell propagating SCWs. These findings were complemented by computer simulations studying the effects of reversal of PLB inhibition in VMs [27,28].

2. Materials and Methods

2.1. Myocyte preparation

The study protocols were approved by the Institutional Animal Care and Use Committee of the Indiana University School of Medicine and the Methodist Research Institute, Indianapolis, Indiana. Hearts from adult C57Bl/6 mice were quickly excised by thoracotomy and retrogradely perfused on a Langendorff apparatus maintained at 37 °C. The enzyme digestion step consisted of perfusing Tyrode's solution containing 1 mg/ml collagenase (Type II, 300 U/mg; Worthington) and 0.1 mg/ml protease (Type XIV, ≥3.5 U/mg; Sigma) for 6 min. Ventricular myocytes (VMs) were dissociated from digested ventricles by gentle mechanical dissociation and used within 3 h. The modified Tyrode's solution contained (in mM) 136 NaCl, 5.4 KCl, 0.33 NaH_2PO_4, 1.0 $MgCl_2$, 10 HEPES, and 10 glucose, pH 7.4 (NaOH) [27]. All chemicals were obtained from Sigma unless indicated otherwise.

2.2. Myocyte permeabilization

VM membranes were permeabilized with saponin (0.005% w/v) for 60 s in a mock internal solution composed of (in mM) 100 potassium aspartate, 20 KCl, 10 HEPES, 0.5 EGTA, and 0.75 $MgCl_2$, pH 7.2 (KOH). Permeabilized VMs were then resuspended in a saponin-free mock internal solution composed of (in mM) 100 potassium aspartate, 20 KCl, 5 KH_2PO_4, 5 MgATP, 10 phosphocreatine, 5 U/ml creatine phosphokinase, 10 HEPES, 0.5 EGTA, 1 $MgCl_2$ (free), 0.015 Fluo-4 (Invitrogen), and 8% w/v dextran (molecular weight ~40,000; to prevent osmotic swelling), pH 7.2 (KOH) [27]. $CaCl_2$ was added to make free [Ca^{2+}] of 50 nM to 1 μM. Free Ca^{2+} concentration and Mg^{2+} concentration were calculated with the use of WebMaxC Extended (maxchelator.stanford.edu). All experiments were performed at room temperature.

2.3. Fab fragment of 2D12 antibody and labeling

Fab fragment of affinity-purified 2D12 was made using a commercial kit (Pierce). In some experiments, 2D12 and Fab were covalently labeled with Alexa-594 (Invitrogen).

2.4. Ca^{2+} spark/wave imaging and immunostaining imaging of the confocal microscopy

We imaged spontaneous Ca^{2+} activity by using the Leica TCS SP8 LSCM inverted microscope fitted with a ×40 1.42 NA oil immersion objective. The Ca^{2+} indicator dye Fluo-4 was excited at 488 nm wavelength with an argon/krypton laser with intensity attenuated to 1–3%. Emission wavelengths >510 nm were detected by the photomultiplier. Fluorescence intensity space–time recordings were acquired in the line-scan mode (1.69 ms/line, 3000 lines/recording) along the longitudinal axis of the myocyte and digitized into 1024 × 1024 pixel images (8-bit) line-scan with nominal pixel dimensions of 98 nm. In some experiments, permeabilized VMs incubated in an internal solution with Fluo-4 were stained with Fab or 2D12 label with Alexa Fluor 594 nm at a concentration of 20 μg/mL for one hour. Samples were then directly examined by microscopy using the ×40 1.42 NA oil immersion objective and a pixel size of 138 nm. The immuno-histological images of Fab-PLB or 2D12-PLB label with Alexa Fluor 594 nm were obtained by illumination with 561 nm laser light, while fluorescence was collected in the long-pass range of >580 nm by the photomultiplier.

2.5. Ca^{2+} spark detection and analysis

The SparkMaster plug-in for ImageJ software [29] was used to detect and analyze Ca^{2+} sparks. The analysis parameters were as follows: scanning speed, 520.8 lines/s; pixel size, 0.08–0.13 μm; spark threshold criteria, 3.8; background, 550–1330; and analysis intervals, 5 [27]. We measured Ca^{2+} spark cluster sizes (spatial widths in line-scan) using a custom algorithm that defines a Ca^{2+} spark cluster as Ca^{2+} sparks separated by less than the single spark average full-width in space and the single spark average full duration in time.

2.6. Ca^{2+}-ATPase assay

Ca^{2+}-dependent ATPase activities of canine SR membranes were measured using an enzyme-coupled spectrophotometric assay [26]. The rate of NADH decay was measured at 340 nm in a SPECTRAmax® PLUS (Molecular Devices) microplate spectrophotometer at 37 °C with 2 μg of membrane protein in buffer containing 50 mM MOPS (pH 7.0), 3 mM $MgCl_2$, 100 mM KCl, 5 mM NaN_3, 3 μg/ml of the Ca^{2+} ionophore A23187, 3 mM ATP, and Ca^{2+}/EGTA as indicated. Ca^{2+}-ATPase activities were measured in the presence and absence of anti-PLB monoclonal antibody 2D12 or the Fab fragment of 2D12. All ATPase activities reported are Ca^{2+}-dependent.

2.7. Computational simulation

We used a VM Ca^{2+} cycling model to simulate the Ca^{2+} sparks and waves in VMs with PLB inhibition [30]. In brief, the model is a three-dimensional Ca^{2+} release unit (CRU) network (65 × 27 × 11 = 19,305 CRUs) with the CRUs coupled via Ca^{2+} diffusion in the myoplasmic space and SR. Each CRU contains a cluster of 100 RyR channels, which were simulated using random Markov transitions. All simulations were

carried out by clamping the membrane voltage at −80 mV. $[Ca^{2+}]_o$ = 10 mM was used to overload the cell to promote Ca^{2+} waves. To simulate the effect of PLB inhibition by Fab, the K_{Ca} of the SR uptake was reduced. Computer simulations were performed on a single NVIDIA Tesla C2050 high-performance Fermi-based graphics-processing unit. Details regarding the numerical algorithms and implementation computing can be found in our recent publication [31].

2.8. Statistics

Data were expressed as means ± SEM. The statistical significance was evaluated by *t*-test and analysis of variance (ANOVA) followed by Bonferroni post hoc tests. A value of $P < 0.05$ was considered statistically significant.

3. Results

3.1. Characterization of Fab fragment of 2D12

Compared to the absence of antibody (Con, *squares*), both Fab (+*Fab, triangles*) and 2D12 (+*2D12, circles*) shifted the Ca^{2+}-activation curve of the Ca^{2+}-dependent ATPase activity of cardiac SR membranes to the left, decreasing the K_{Ca} value from 0.30 ± 0.04 μM to 0.15 ± 0.03 μM and 0.11 ± 0.02 μM ($n = 6$, $P = 0.02$ compared to control), respectively (Fig. 1A), thus restoring the high apparent Ca^{2+} affinity of the Ca^{2+} pump. These results suggest that the Fab, similar to the well- studied 2D12 [26], almost completely reversed PLB inhibition. Fab increased the Ca^{2+}-ATPase activity more than 2-fold at low free Ca^{2+} concentrations (from ~50 to ~200 nM) as compared to the absence of PLB inhibition. However, Fab did not affect the maximal enzyme velocity of Ca^{2+}-ATPase activity at saturating Ca^{2+} concentrations. Similar results were obtained when Ca^{2+} uptake by SR vesicles was measured (data not shown).

We tested the binding efficacy of Fab or 2D12 to PLB in permeabilized, semi-intact VMs. Fab or 2D12, covalently labeled with Alexa-594 (20 μg/ml), was added directly to the bath and permeabilized VMs were imaged with confocal microscopy (Fig. 1B). After 15 min of antibody incubation, we found strong immunofluorescent signals showing a characteristic cross-striated staining pattern at about 2 μm intervals, suggesting that Fab penetrated well into permeabilized VMs and efficiently bound to PLB. In contrast, 2D12 fluorescence was usually localized at the periphery of the VMs and did not penetrate deep into VMs. In control experiments, we incubated permeabilized VMs with Fab (covalently labeled with Alexa-594) and peptide containing PLB residue 1–31. As shown in Fig. 1G, PLB1-31 completely blocked Fab binding to PLB, confirming the high specificity of Fab binding to PLB. In addition, co-incubation with Fab (covalently labeled with Alexa-594) and the monoclonal anti-SERCA2a antibody 2A7-A1 (covalently labeled with Alexa-488) revealed co-localization of signals, consistent with the close proximity of the two proteins (Fig. 1H to J). These results suggest that Fab, as compared to the 2D12, is a better reagent for penetrating into the SR myocytes, and binds to native PLB more completely in the SR membrane of permeabilized VMs.

3.2. Effect of Fab on Ca^{2+} sparks/SCWs

We next studied how Fab binding to PLB affects intracellular Ca^{2+} cycling in VMs. Fig. 2 shows confocal images of Ca^{2+} fluorescence from the Fluo-4 Ca^{2+} indicator and immunofluorescence from Fab in the same permeabilized VM before and after the addition of Alexa-594-labeled Fab. At the baseline, 50 nM free $[Ca^{2+}]$ generated multiple Ca^{2+} sparks (Fig. 2A, *left panel*), which is consistent with the results of previous studies [16]. Approximately 15 min after Fab incubation, Ca^{2+} spark clusters and mini-waves increased significantly (from 0.7 ± 0.1 to 1.9 ± 0.8 Hz) (Fig. 2A, *middle panel*). The background Ca^{2+} signal decreased, which may result from a transient reduction in cytosolic Ca^{2+} by increased SERCA2a uptake until a new leak–uptake balance is reached for SR. At the same time, Fig. 2B and C show the development of strong immunofluorescent signals from Alexa-594-labeled Fab in the same VM, confirming that PLB was bound efficiently by Fab (Fig. 2C). Furthermore, the SERCA inhibitor, thapsigargin (10 μM), completely abolished Ca^{2+} sparks and clusters (Fig. 2A, *right panel*). These results suggest that Fab binding to PLB reverses its inhibition of SERCA2a. As a result, higher SR Ca^{2+} contents caused increased spontaneous SR Ca^{2+} release events.

cAMP activates PKA, leading to phosphorylation of PLB at Ser16 and reversal of PLB inhibition (Supplementary Figure S1), thus augmenting SR Ca^{2+} content and spontaneous Ca^{2+} release [3,24,32]. We used the cAMP response as a control to verify the extent of the Fab effect. We sequentially added cAMP before or after Fab or 2D12 addition to myocytes. Fig. 3A shows that with 200 nM free $[Ca^{2+}]$, 2D12 only slightly increased the frequency of Ca^{2+} sparks but did not generate SCW,

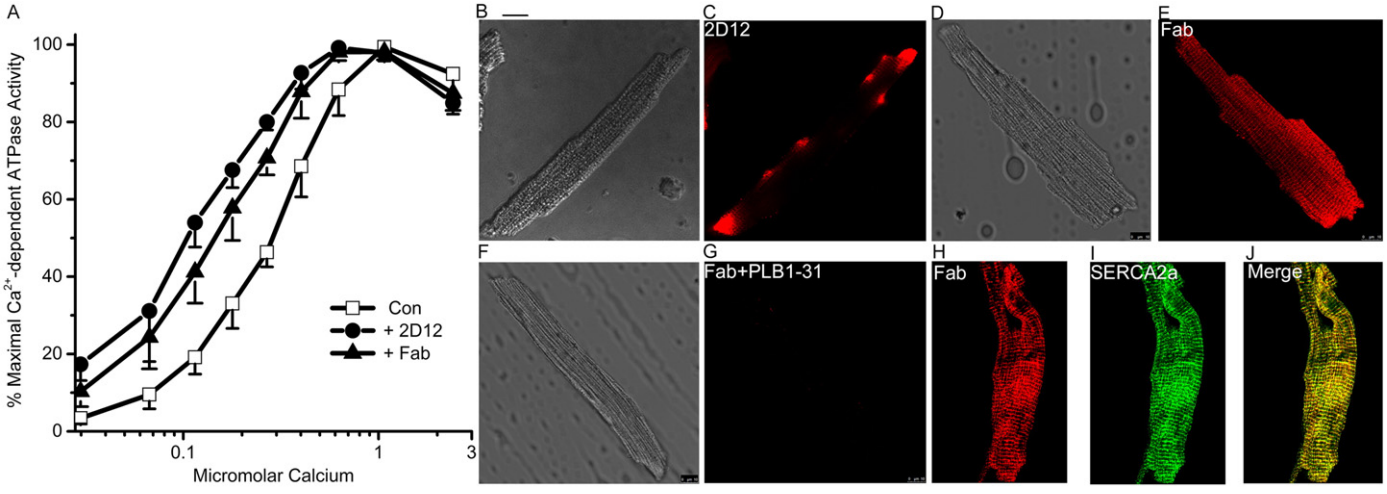

Fig. 1. Fab binding to native PLB. (A) The effect of Fab or 2D12 on the Ca^{2+}-dependent ATPase activity of cardiac SR membranes. Six experiments were performed. See text for K_{Ca} values. (B–G) Representative confocal immunofluorescence images showing binding of Fab or 2D12 to PLB in permeabilized VMs. A total of 20 μg/ml Alexa-594 labeled 2D12 (*B* and *C*) or Fab (*D* to G) was added to permeabilized VM and incubated for 15 min at room temperature. A peptide containing PLB residue 1–31 was incubated with Fab-594 in experiments in Fig. 1F and G. H to J, fixed VMs were co-incubated with Fab (covalently labeled with Alexa-594) and the monoclonal anti-SERCA2a antibody 2A7-A1 (covalently labeled with Alexa-488). Overlay image was shown in Fig. 1J. Images were obtained under the DIC (B, D, and F) and fluorescent (C, E, and G–J) mode of confocal microscopy, respectively. Bar represents 10 μm.

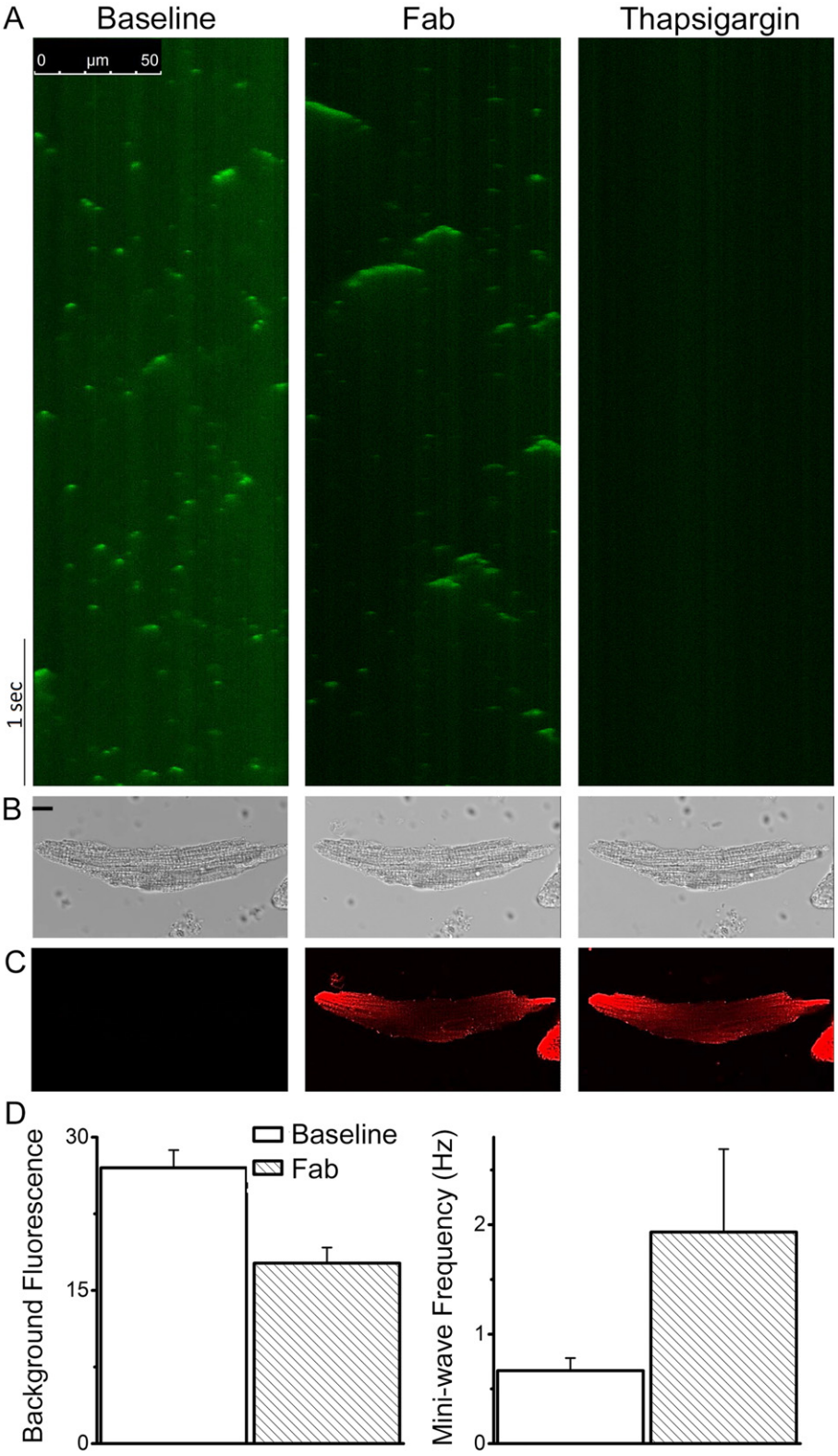

Fig. 2. Confocal Ca^{2+} and immunofluorescence imaging of a representative permeabilized VM. The Ca^{2+} activity with Fluo-4 Ca^{2+} indicator and PLB immunostaining by Fab covalently labeled with Alexa-594 in VMs were measured under the line-scan mode (A), DIC (B), or fluorescence mode (C) of a confocal microscope at baseline (*left panels*), 15 min after antibody incubation (*middle panels*), and after thapsigargin (*right panels*) (10 μM) consecutively. (D) Bar graphs showed the background fluorescence and the number of Ca^{2+} clusters and mini-waves before and after the addition of Fab ($n = 3$ cells, $P < 0.05$). The free [Ca^{2+}] in the bath was 50 nM.

consistent with the findings of Sirenko *et al.* [24]. However, 20 μM cAMP following 2D12 incubation caused a transition from stochastic Ca^{2+} sparks to periodic and whole-cell SCWs, consistent with the previously reported effect of cAMP [24]. Importantly, as shown in Fig. 3B, Fab alone changed the Ca^{2+} activity from sparks/macrosparks into periodic and whole-cell propagating SCWs. Sequential addition of cAMP had little effect on the morphology or frequency of SCW in the VMs already treated with Fab (Fig. 3B, *right panel*). In separate experiments in which we

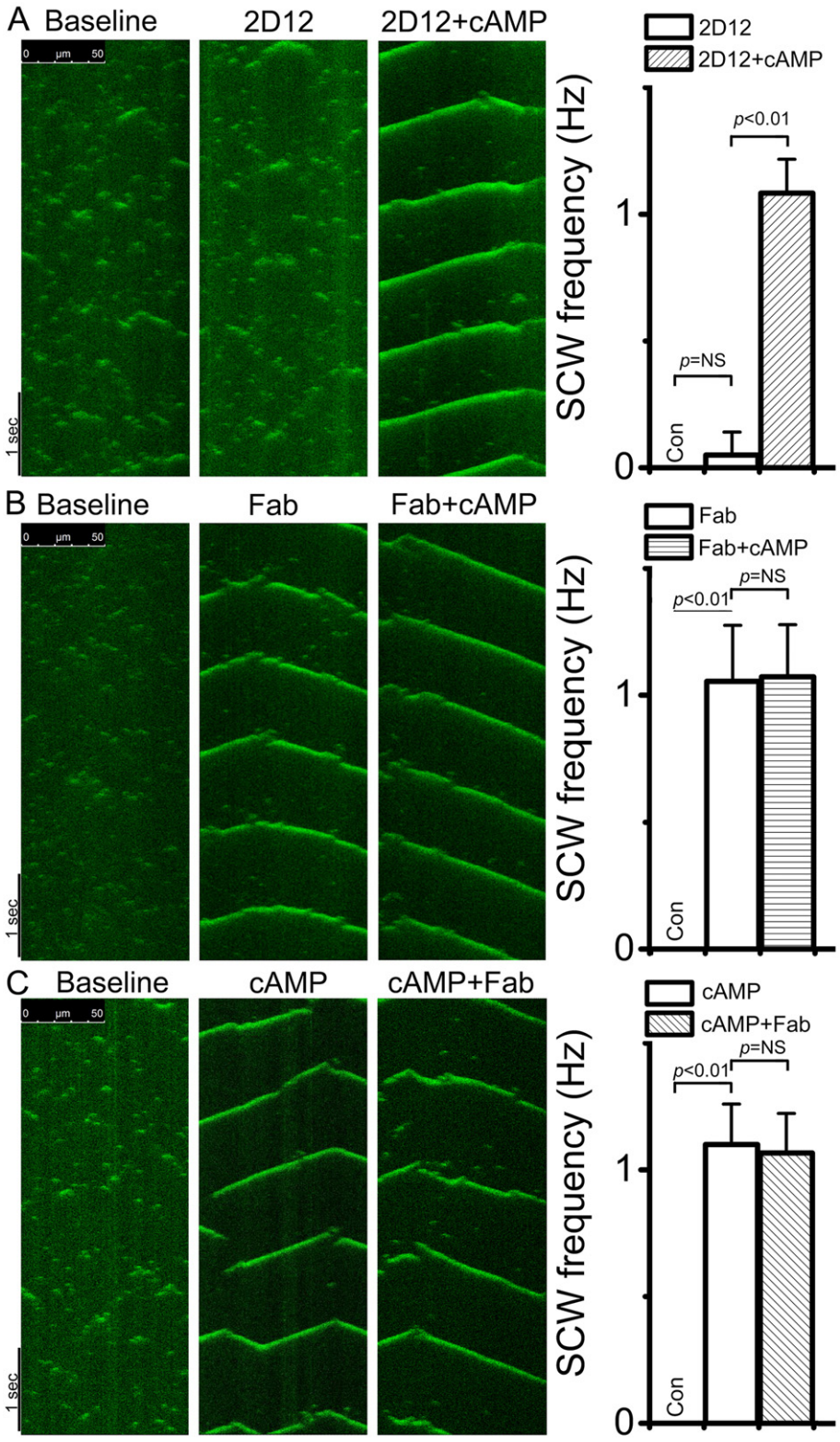

Fig. 3. The effect of 2D12 or Fab on the intracellular Ca^{2+} activity in the permeabilized VM. Confocal Ca^{2+} imaging of permeabilized VMs was obtained with the Fluo-4 Ca^{2+} indicator under the line-scan mode. The baseline (*left panels*) was recorded in 200 nM free [Ca^{2+}]. Antibody (100 μg/ml) or cAMP (20 μM) was added sequentially to the bath as indicated (*top*). (A) Ca^{2+} activity in a VM after 15 min of incubation with 2D12, and then after cAMP. (B) Ca^{2+} activity in a VM after 15 min of incubation with Fab, and then after cAMP. (C) Ca^{2+} activity in a VM after 15 min of incubation with cAMP, and then after Fab. Plots were averages of at least 10 VMs.

added cAMP first, the addition of Fab had no further effect on SCWs generated by cAMP (Fig. 3C). The above results demonstrate that Fab, which specifically dissociates PLB from the SERCA2a and reverses PLB inhibition, dramatically increases spontaneous Ca^{2+} release in VMs. Again, due to its poor binding efficiency in permeabilized VMs, 2D12 only marginally altered intracellular Ca^{2+} dynamics. These experiments show for the first time that acute elimination of PLB inhibition itself is sufficient to facilitate the formation of SCWs in VMs.

The specificity of Fab in the dose- and time-dependent effect on spontaneous subcellular Ca^{2+} releases was further studied in VMs.

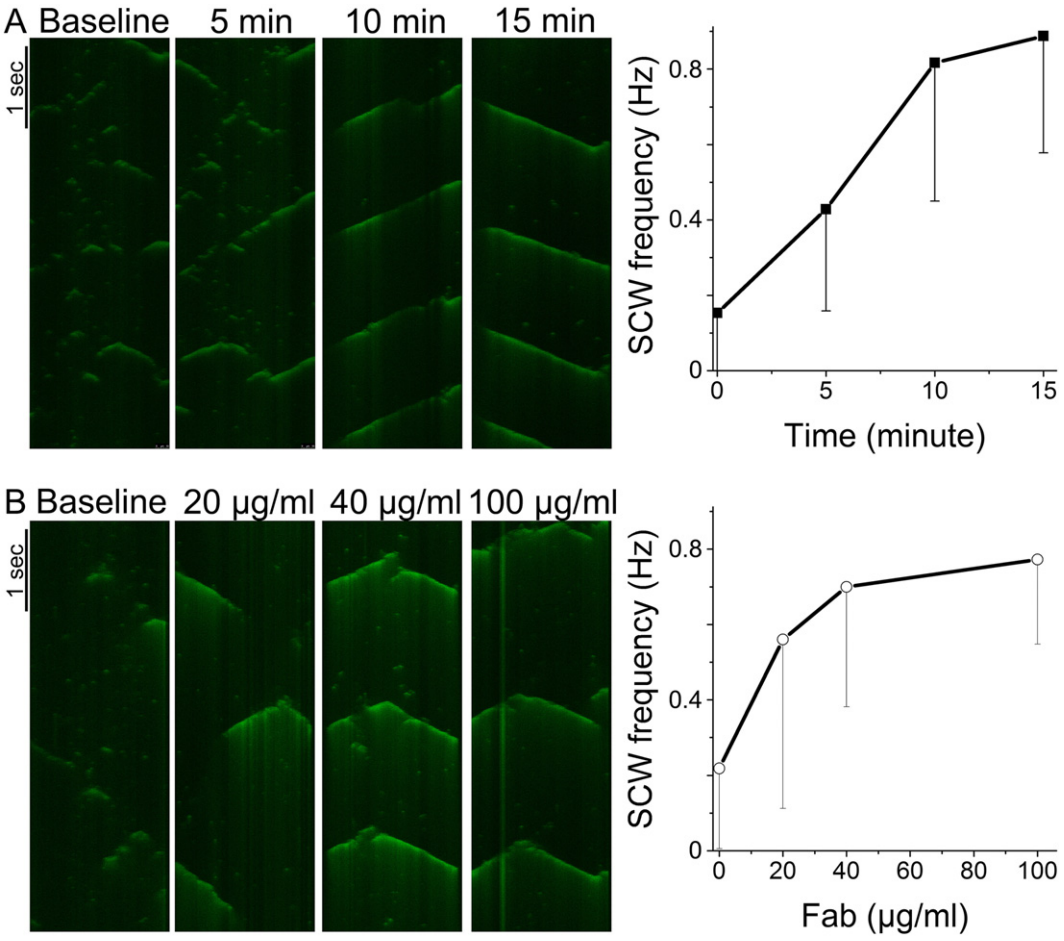

Fig. 4. Time- and dose-dependent effects of Fab on intracellular Ca^{2+} activity. Confocal Ca^{2+} imaging of permeabilized VMs used Fluo-4 Ca^{2+} indicator under the line-scan mode. Baseline was obtained in the absence of Fab under the free [Ca^{2+}] of 200 nM. (A) Ca^{2+} images were obtained at various time points (*top*) after Fab exposure (100 μg/ml). (B) Ca^{2+} images were obtained after the addition of Fab sequentially (*top*) at a time interval of 15 min. Plots were averages of at least 4 VMs.

Fig. 4A shows the time course of the XT line-scan of a VM exposed to 200 nM of free [Ca^{2+}] after the addition of Fab (100 μg/ml). In 5 min, the Ca^{2+} activity evolved from small Ca^{2+} sparks at baseline into chains of Ca^{2+} clusters with increased amplitude, temporal and spatial spread. Fifteen minutes after the addition of Fab, periodic and organized SCWs propagated over the entire VM (Fig. 4A). In addition, Fig. 4B shows the time interval of 15 min after Fab was gradually titrated up in the cell suspension. As exposure concentration of Fab increased, the Ca^{2+} activity evolved from rare small Ca^{2+} spark clusters at baseline into chains of Ca^{2+} sparks and SCWs. The maximal effect of Fab was saturated after 40 μg/ml. In control experiments, the addition of affinity-purified monoclonal anti-SERCA2a antibody, 2A7-A1, which was purified in the same buffer as for 2D12, had no effect on the spontaneous subcellular Ca^{2+} release activity over 1 h (data not shown).

3.3. The Ca^{2+}-dependency of Fab effect in VMs

We recorded the local Ca^{2+} release in the XT line-scan in permeabilized VMs before and after Fab application (100 μg/ml) at different free [Ca^{2+}] (Fig. 5). In each experiment, cAMP (20 μM) was added into the cell suspension 30 min after Fab application to test for any further change in local Ca^{2+} release. At 50 nM free [Ca^{2+}], there were multiple stochastic spontaneous Ca^{2+} sparks in VMs at baseline (Fig. 5A). After Fab application, the frequency of Ca^{2+} sparks was increased about 1.5-fold from 11.3 ± 5.4 sparks s^{-1} $(100\ \mu m)^{-1}$ at baseline to 17.1 ± 4.8 sparks s^{-1} $(100\ \mu m)^{-1}$ ($n = 12$, $P = 0.002$). In addition, macrosparks and mini-waves were noted after Fab administration (Fig. 5A). The properties of the Ca^{2+} sparks at baseline and after Fab are summarized in Table 1. In particular, the amplitude of sparks increased from 1.7 ± 0.4 in F/F_0 at baseline to 2.9 ± 0.8 in F/F_0 ($P = 0.002$); the full-width at half-maximal amplitude (FWHM) increased from 2.2 ± 0.3 to 2.4 ± 0.3 μm ($P = 0.04$); the full duration at half-maximal amplitude (FDHM) increased from 20.5 ± 3.4 to 23.3 ± 3.4 ms ($P = 0.002$). There were no differences in the time constant of Ca^{2+} spark decay between the baseline vs Fab administration. cAMP (20 μM) after Fab application did not further change the frequency or morphology of Ca^{2+} sparks (Fig. 5A and Table 1). All these results suggest that Fab inhibition of PLB increased the frequency and magnitude of local Ca^{2+} release.

With physiological diastolic free [Ca^{2+}] of 100 and 200 nM in permeabilized VMs at baseline, there were multiple Ca^{2+} sparks but no whole-cell SCW (Fig. 5B and C, panel *a*). After Fab administration, periodic SCWs formed and propagated in the whole-cell ($P < 0.001$). Table 2 shows characteristics of SCWs. Again, it should be noted that the formation of SCWs was accompanied by a significant reduction in background fluorescence, consistent with increased SR Ca^{2+} uptake and lowered cytoplasmic Ca^{2+} concentration after adding Fab (compare traces *b* to *a* in Fig. 5B and C). At 400 nM free [Ca^{2+}], Fab converted the fractured partial organized SCWs at baseline into highly synchronized and organized SCWs (Fig. 5D). Further, in addition to increasing the amplitude (2.9 ± 0.3 vs 4.4 ± 0.4 in F/F_0, $P < 0.001$) and shortening the Ca^{2+} decay time of SCWs from 89 ± 14 to 52 ± 8 ms after Fab addition ($P < 0.001$, Table 2), Fab significantly increased the frequency of the SCWs from 1.1 ± 0.4 to 1.6 ± 0.5 Hz ($P = 0.001$) (compare traces *b* to *a* in Fig. 5D). At 500 nM free [Ca^{2+}], there were already periodic and organized SCWs in the VMs at baseline (Fig. 5E, panel a). As expected,

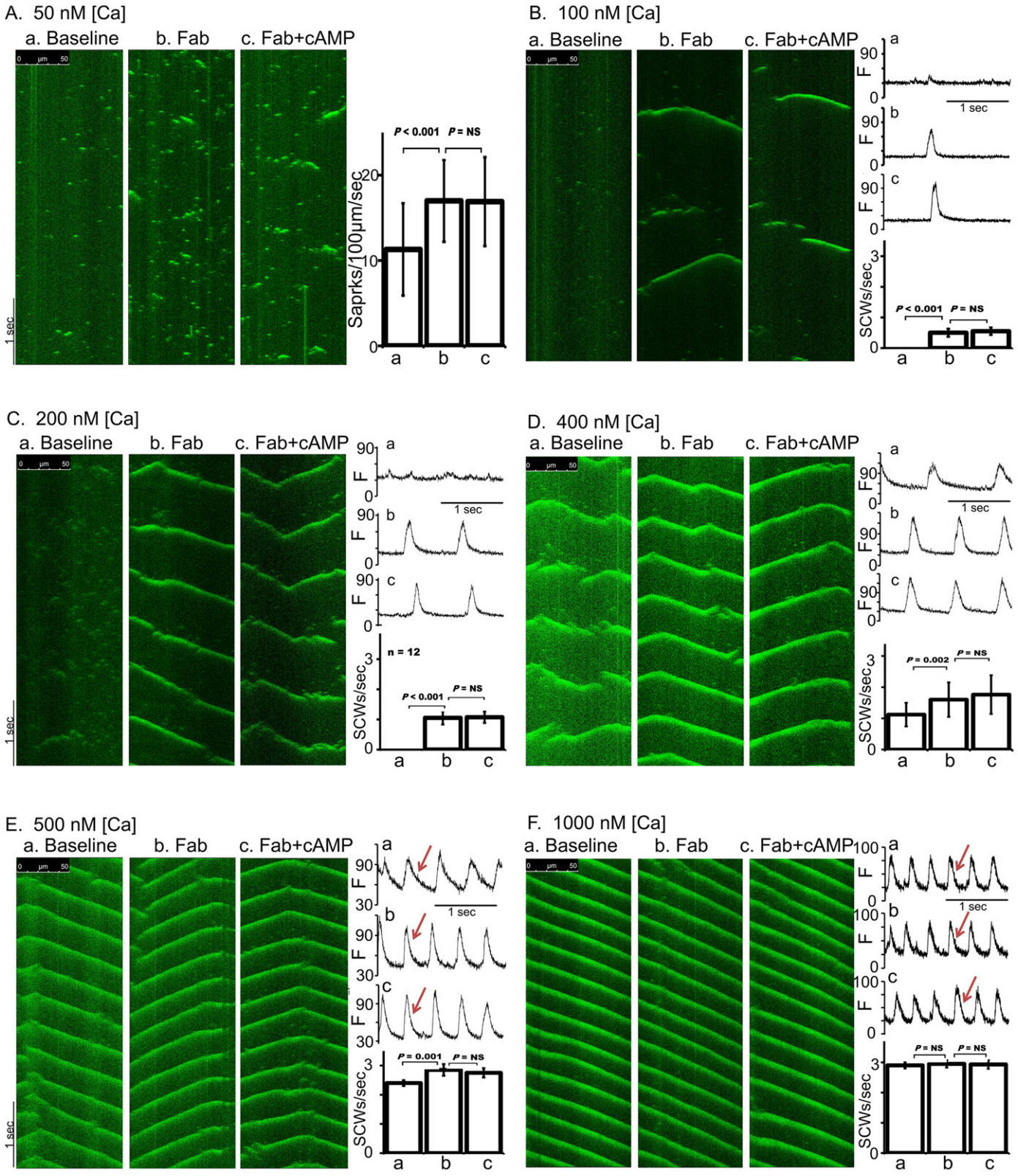

Fig. 5. Effect of Fab on the intracellular Ca^{2+} activity at various Ca^{2+} concentrations. (A–F) At each Ca^{2+} concentration indicated ([Ca]), confocal line-scan images of the same permeabilized VM were obtained at baseline (a), after the addition of 100 μg/ml Fab (b), and after 20 μM cAMP (c) exposure consecutively. Bar graphs showed the frequency of Ca^{2+} sparks or waves at each condition. *P* value was indicated. Traces in B to F showed intensity of fluorescent signals (*F*) of SCWs. See Table 2 for the Ca^{2+} decay time and velocity of SCWs (as arrows). At least 12 VMs were imaged at each condition.

Fab decreased the Ca^{2+} decay time of SCWs from 74 ± 12 to 54 ± 4 ms after Fab addition ($P < 0.001$, Fig. 5E, *red arrows*), which is consistent with the idea that relief of PLB inhibition of SECA2a by Fab speeds up Ca^{2+} uptake. Importantly, Fab further increased the frequency of SCWs from 2.4 ± 0.1 at baseline to 2.8 ± 0.2 Hz, $P < 0.001$) (Fig. 5E). In addition, Fab increased SCW velocity at these Ca^{2+} concentrations.

Table 1
Ca^{2+} spark characteristics.
Ca^{2+} sparks were measured in permeabilized VMs at 50 nM free [Ca^{2+}] as indicated in Fig. 5. Ca^{2+} sparks characteristics at baseline, after Fab (100 μg/ml), and after cAMP (20 μM) are reported. Total number of Ca^{2+} sparks, amplitude, FWHM, FDHM, and the Ca^{2+} decay time of Ca^{2+} sparks (Tau decay) were compared using one-way ANOVA ($n = 12$; *, baseline vs Fab, $P < 0.05$; $^{+}$, baseline vs cAMP, $P < 0.05$). Data are mean ± SEM.

	Total spark number	Peak amplitude (F/F_0)	FWHM (μm)	FDHM (ms)	Tau decay (ms)
Baseline	678	1.8 ± 0.4	2.2 ± 0.3	20.5 ± 3.4	20.4 ± 4.4
Fab	1020	2.9 ± 0.8*	2.4 ± 0.3*	23.3 ± 3.3*	22.3 ± 7.9
cAMP	1014	2.8 ± 0.9^{+}	2.4 ± 0.4^{+}	23.8 ± 3.5^{+}	22.0 ± 8.1

At 1000 nM free [Ca^{2+}], there was no significant difference in the frequency, velocity, or Ca^{2+} decay of SCWs between the baseline and after Fab application (Fig. 5F, *red arrows*), compatible with the finding that PLB inhibition did not affect maximal Ca^{2+}-ATPase activity in native SR vesicles at high micromolar free [Ca^{2+}] (Fig. 1A). Finally, for all free [Ca^{2+}] concentrations tested, sequential addition of cAMP (20 μM) 30 min after Fab application did not further change the frequency or morphology of SCWs in VMs (Fig. 5, panel *c*), respectively.

3.4. The computational modeling of the effects of reversal of PLB inhibition on Ca^{2+} cycling dynamics

To investigate whether Fab reversal of PLB inhibition alone can promote Ca waves, we carried out computer simulations using a VM model under Ca^{2+} overload condition for different K_{Ca} of the SERCA pump. Fig. 6 shows the computer simulation results of the effects of PLB inhibition on Ca^{2+} waves and oscillations. When $K_{Ca} > 0.5$ μM (Fig.6A), the VMs predominantly exhibited single sparks, spark clusters, and miniwaves. As K_{Ca} was decreased to simulate reversal of PLB inhibition, more and more spark clusters and non-persistent waves form. At $K_{Ca} =$ 0.35 μM (Fig. 6B), persistent Ca^{2+} waves and periodic whole-cell Ca^{2+} oscillation occurred. As K_{Ca} was decreased further, the whole-cell Ca^{2+} oscillations became more periodic and the period decreased (compare Fig.6B and C). As shown in the bottom panels in Fig. 6, decreasing K_{Ca} increased the SR load, which is the dominant cause promoting Ca waves and oscillations in the simulations. These results are fully consistent with the experimental findings observed in the murine VMs.

4. Discussion

This present study shows that acute specific reversal of PLB inhibition by the anti-PLB monoclonal antibody had a significant impact on the subcellular Ca^{2+} activity in normal VMs. The experimental results and computational simulations demonstrate that reversal of PLB inhibition alone, with or without activating RyR2, was sufficient to initiate cell-wide SCWs in isolated permeabilized murine VMs.

4.1. New platform to investigate PLB in influencing subcellular Ca^{2+} activity

Animal models (e.g., PLB-KO mice) provide valuable tools to study the relationship between PLB and subcellular Ca^{2+} activity. However, the chronic PLB-KO mouse model is associated with compensatory adaptations. In particular, in response to the chronically elevated Ca^{2+} contents in the SR in PLB-KO mouse, RyR2 expression is reduced by 30% [20]. Therefore, the SR Ca^{2+}-release process in PLB-KO mice is altered, which makes it difficult to determine whether the observed phenotype is due to loss of PLB alone or to the accompanying compensatory mechanisms [20].

Pharmacological interventions have been used to study the effects of PLB inhibition, but these drugs may have off-target effects. For example, studies of the actions of PLB on the spontaneous SR Ca^{2+} release are complicated at the cellular level when using protein phosphatase inhibitor, cAMP, or kinase itself to activate PKA or CaMKII. Because these interventions simultaneously target multiple proteins (e.g. RyR2, dihydropyridine receptors, CaMKII, PLB) that affect intracellular Ca^{2+} dynamics and cellular function, it is not possible to define a specific role for PLB in intracellular Ca^{2+} handling.

Biochemical studies have demonstrated that the intact monoclonal antibody, 2D12, specifically reversed SERCA2a inhibition by completely disrupting PLB binding to SERCA2a in native SR vesicles [26,33]. However, delivering 2D12 into living VMs remains challenging. Sham *et al.* used patch pipette to inject 2D12 into intact VMs and demonstrated that 2D12 reversed SERCA2a inhibition in VMs and mimicked the effects induced by β-adrenergic stimulation on the Ca^{2+} transient, without any notable cytotoxicity or off-target effect [5]. Alternatively, saponin-permeabilized VMs provide a semi-intact system, allowing direct access of protein/reagents to the intracellular space [34]. Recently, Sirenko *et al.* reported that the addition of 2D12 to permeabilized rabbit VMs induced a self-organized and partial synchronization of spontaneous Ca^{2+} releases [24]. However, being a relatively large-sized molecule of ~150 KD, 2D12 apparently has difficulty passing through the discrete pores of 30 Å diameter in permeabilized VMs created by saponin [35,36], which is shown in our study (Fig. 1). Here, we used the Fab fragment of 2D12, which is only ~1/3 the size of 2D12, to achieve deeper penetration and more efficient binding to PLB, and observed robust effects on subcellular Ca^{2+} activity in VMs (Figs. 1 to 3).

Specifically, Fab binding to PLB was directly monitored by immunofluorescent signals from the covalently labeled Alexa-594 fluorophore and correlated to increased intracellular Ca^{2+} release (Fig. 2). Also, the dose- and time-dependent changes of subcellular Ca^{2+} activity confirmed the specificity of Fab. To achieve the maximal reversal of PLB inhibition, we used a saturating dose of Fab (~100 μg/ml) in our experiments. Efficient Fab binding to PLB was verified by a strong correlation in Ca^{2+}-dependency (i.e., large effect at low physiology concentration, small effect at high intracellular Ca^{2+} concentrations) between the effect of Fab on intracellular Ca^{2+} kinetics at the subcellular level and on Ca^{2+}-ATPase enzyme activity in *in vitro* studies. A significant decrease in SCWs decay time

Table 2
Spontaneous Ca^{2+} wave characteristics.
Spontaneous Ca^{2+} wave (SCWs) were measured in permeabilized VMs at various free [Ca^{2+}] as indicated in Fig. 5. SCWs characteristics at baseline, after Fab (100 μg/ml), and after cAMP (20 μM) are reported. SCWs Ca^{2+} decay time, velocity, frequency, and $\Delta F/F_0$ were compared using one-way ANOVA (12 cells from 4 mice were chosen for comparison in each free [Ca^{2+}], *, baseline vs Fab, $P < 0.05$; ^, baseline vs Fab + cAMP, $P < 0.05$). Data are mean ± SEM.

	Decay time (ms)			Velocity (μm/s)			Frequency (Hz)			$\Delta F/F_0$		
Free [Ca^{2+}] (nM)	Baseline	Fab	Fab + cAMP	Baseline	Fab	Fab + cAMP	Baseline	Fab	Fab + cAMP	Baseline	Fab	Fab + cAMP
100	–	44 ± 6*	47 ± 8^	–	133 ± 21*	138 ± 25^	–	0.44 ± 0.16*	0.46 ± 0.13^	–	4.68 ± 0.54*	4.84 ± 0.69^
200	–	45 ± 7*	46 ± 9^	–	140 ± 26*	142 ± 20^	–	1.05 ± 0.21*	1.07 ± 0.21^	–	4.49 ± 0.63*	4.45 ± 0.57^
400	89 ± 14	52 ± 8*	53 ± 9^	112 ± 26	144 ± 13*	146 ± 21^	1.12 ± 0.38	1.61 ± 0.55*	1.76 ± 0.62^	2.89 ± 0.31	4.41 ± 0.41*	4.38 ± 0.38^
500	74 ± 12	54 ± 4*	52 ± 8^	123 ± 10	143 ± 23*	150 ± 25^	2.38 ± 0.11	2.82 ± 0.24*	2.76 ± 0.16^	2.39 ± 0.51	2.91 ± 1.02	2.88 ± 0.71
1000	61 ± 9	60 ± 8	60 ± 9	157 ± 23	156 ± 24	157 ± 24	2.90 ± 0.11	2.95 ± 0.12	2.93 ± 0.14	2.33 ± 0.38	2.38 ± 0.32	2.41 ± 0.34

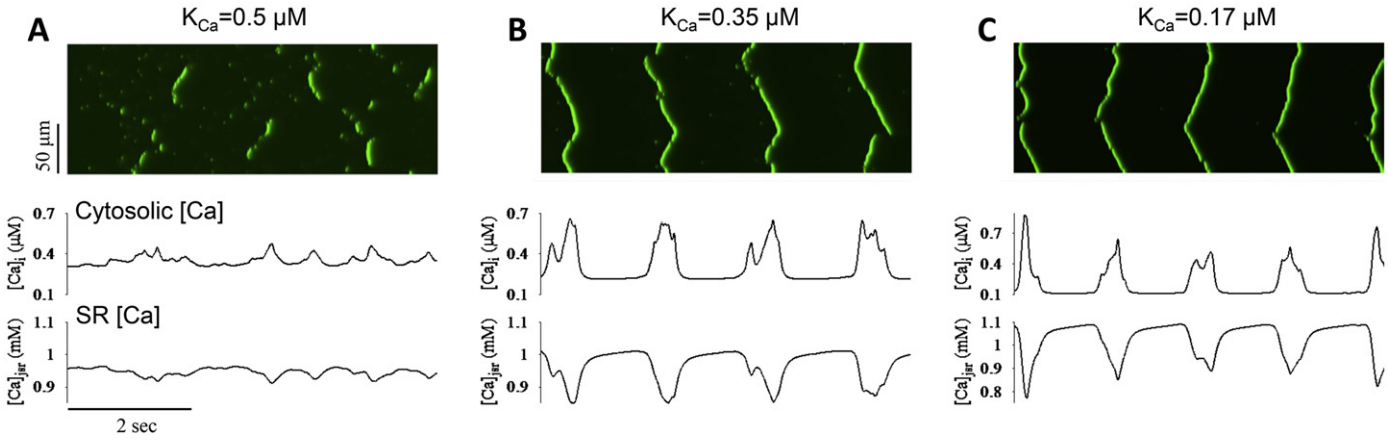

Fig. 6. Computer simulation results of intracellular Ca^{2+} activity under different K_{Ca}. Top panels: space–time plots of cytosolic Ca concentration for K_{Ca} of 0.5 μM (A), 0.35 μM (B), and 0.17 μM (C). Middle panels: whole-cell cytosolic Ca concentrations versus time for the corresponding K_{Ca} values. Bottom panels: whole-cell SR Ca concentrations versus time for the corresponding K_{Ca} values.

at free [Ca^{2+}] below 500 nM after Fab application is consistent with the well characterized effects of reversal of PLB inhibition. High concentrations of cAMP (20 μM) after Fab application did not cause any further change in subcellular Ca^{2+} activity at different baseline levels of free [Ca^{2+}], indicating that PLB is efficiently saturated by Fab and uncoupled from Ca^{2+}-ATPase inhibition. Therefore, Fab appears to be a valuable new tool to selectively reverse PLB inhibition of SERCA2a in permeabilized VMs, and provides an attractive new system to delineate the role of PLB and other factors in the regulation of spontaneous SR Ca^{2+} release.

4.2. PLB is the key regulator in the rhythmic regulation of VMs

PLB is well known to regulate excitation–contraction coupling in heart. Here, by showing that acute reversal of PLB inhibition increased the Ca^{2+} sparks and facilitated the formation of SCWs, we demonstrate that PLB is also a powerful regulator for the formation of rhythmic subcellular Ca^{2+} activity in VMs. Note that reversal of PLB inhibition may affect SCWs in two ways: by enhancing SERCA2a uptake, PLB may buffer the diffusion of Ca^{2+} from the Ca^{2+} release site to the Ca^{2+} release site, leading to less effective Ca^{2+}-induced Ca^{2+} release and broken SCWs; on the other hand, reversal of PLB inhibition also increases Ca^{2+} SR content, leading to greater local Ca^{2+} releases favoring the propagation of SCWs. Further, our data suggest that acute reversal of PLB inhibition increased SCW velocity (Table 2). This phenomenon can be explained by the "sensitization" wave-front hypothesis proposed by Keller *et al.* [37]. Local increase in Ca^{2+} inside SR, by acute reversal of PLB inhibition, may sensitize nearby RyR2 clusters, speeding up SCW propagation. When we modeled the effect of increasing the Ca^{2+} affinity of SERCA2a (decreasing K_{Ca} value), we indeed found that the latter effect predominated and Ca^{2+} waves were promoted, consistent with our experimental data (Figs. 5 and 6).

Our data may also be relevant to observations obtained using the PLB-KO mouse model [38,39]. Unlike our results in which acute removal of PLB inhibition in normal VMs promoted propagating SCWs, quiescent PLB-KO VMs did not exhibit cell-wide propagating SCWs [8,40]. When crossed with RyR2-R4496C mutant mice (a CPVT model), which show increased proclivity to SCWs, the double mutant VMs showed an increased frequency of Ca^{2+} sparks and miniwaves, but did not exhibit whole-cell propagating SCWs, suggesting that the reversal of PLB inhibition might be therapeutic in CPVT. However, it should be noted that in order to compensate the abnormal SR Ca^{2+} homeostasis, PLB-KO mouse downregulates the expression of RyR2 [20], which is expected to inhibit Ca^{2+} wave propagation. In addition, crossing PLB-KO with other mouse models is also known to cause various Ca^{2+} protein adaptations [21]. For example, mice with PLB-KO and SERCA2a replacement by the high Ca^{2+} affinity SERCA2b were shown to develop severe cardiac hypertrophy [41]. Further, Louch *et al.* found that PLB ablation caused further down-regulation of the Ca^{2+} pump in these mice but normalized global Ca^{2+} homeostasis in cardiomyocytes [42]. They suggest that the Ca^{2+} affinity of SERCA plays a more important role than the expression level and maximal turnover rate. Here, we showed that acute reduction in Ca^{2+} affinity of SERCA2a by reversing PLB inhibition, but with intact SERCA2a, caused a significant increase in intracellular Ca^{2+} release, consistent with the importance of PLB modulation of SERCA2a Ca^{2+} affinity in the regulation of intracellular Ca^{2+} dynamics.

PLB is a key modulator of subcellular Ca^{2+} kinetics and may serve as a therapeutic target to improve inotropic function of the heart. Our data here indicates that PLB could also be targeted to induce chronotropic effects. For example, as a potential future direction of bio-pacemaker design [24], selective reversal of PLB inhibition could initiate rhythmic whole-cell propagating Ca^{2+} activity, i.e., a "Ca^{2+} clock" under physiological diastolic [Ca^{2+}] conditions (i.e. 100 nM in our study) in quiescent VMs. On the other hand, while selective PLB inhibition provides a potentially promising way to enhance the SERCA2a activity and restores the normal SR Ca^{2+} load in patients with heart failure, the same intervention may potentially increase the risk of trigger activity or automaticity, leading to ventricular arrhythmia in the acute phase.

5. Limitations

The present studies were performed at room temperature, which affects the rate of SERCA2a activity. However, previous experiments with permeabilized myocytes were also usually performed at room temperature [16,17]. The SR Ca^{2+} content was not estimated in the study. We used the effect of cAMP as a positive control. We used permeabilized rather than intact VMs for these experiments. Permeabilization may cause lost accessory proteins or factors required for phosphorylation. Although similar results were obtained in intact and permeabilized VMs in previous studies [16,17,34], whether the results in permeabilized VMs can be directly extrapolated to intact myocytes is untested. To minimize this limitation, we also performed computer simulation studies using an intact VM model. There are differences between K_{Ca} values used in simulation using a whole cell model and in *in vitro* experiments using pure membranes in the test tubes (Fig. 1). Different K_{Ca} values were used in various simulation approaches in the literature. Because the results were consistent with those obtained with permeabilized VMs, these simulation studies strengthen the conclusions of our study.

Disclosures

None.

Funding Source

This study was supported in part by NIH Grants R37-HL049428 (LRJ), P01 HL78931 (JNW), R0171140, a Medtronic-Zipes Endowment (PSC), the Indiana University Health-Indiana University School of Medicine Strategic Research Initiative and the Kawata and Laubisch endowments of the UCLA.

Acknowledgments

We thank Jin Guo, Glen A. Schmeisser, and Jian Tan for the technical support.

Appendix A. Supplementary data

Supplementary data to this article can be found online at http://dx.doi.org/10.1016/j.yjmcc.2014.12.024.

References

[1] Simmerman HK, Jones LR. Phospholamban: protein structure, mechanism of action, and role in cardiac function. Physiol Rev 1998;78:921–47.
[2] Kranias EG, Hajjar RJ. Modulation of cardiac contractility by the phospholamban/SERCA2a regulatome. Circ Res 2012;110:1646–60.
[3] Lindemann JP, Jones LR, Hathaway DR, Henry BG, Watanabe AM. beta-Adrenergic stimulation of phospholamban phosphorylation and Ca^{2+}-ATPase activity in guinea pig ventricles. J Biol Chem 1983;258:464–71.
[4] Brittsan AG, Kranias EG. Phospholamban and cardiac contractile function. J Mol Cell Cardiol 2000;32:2131–9.
[5] Sham JS, Jones LR, Morad M. Phospholamban mediates the beta-adrenergic-enhanced Ca^{2+} uptake in mammalian ventricular myocytes. Am J Physiol 1991;261:H1344–9.
[6] Mattiazzi A, Hove-Madsen L, Bers DM. Protein kinase inhibitors reduce SR Ca transport in permeabilized cardiac myocytes. Am J Physiol 1994;267:H812–20.
[7] Luo W, Grupp IL, Harrer J, Ponniah S, Grupp G, Duffy JJ, et al. Targeted ablation of the phospholamban gene is associated with markedly enhanced myocardial contractility and loss of beta-agonist stimulation. Circ Res 1994;75:401–9.
[8] Santana LF, Kranias EG, Lederer WJ. Calcium sparks and excitation-contraction coupling in phospholamban-deficient mouse ventricular myocytes. J Physiol 1997;503(Pt 1):21–9.
[9] Wolska BM, Stojanovic MO, Luo W, Kranias EG, Solaro RJ. Effect of ablation of phospholamban on dynamics of cardiac myocyte contraction and intracellular Ca^{2+}. Am J Physiol 1996;271:C391–7.
[10] Koss KL, Kranias EG. Phospholamban: a prominent regulator of myocardial contractility. Circ Res 1996;79:1059–63.
[11] Eisner DA, Kashimura T, O'Neill SC, Venetucci LA, Trafford AW. What role does modulation of the ryanodine receptor play in cardiac inotropy and arrhythmogenesis? J Mol Cell Cardiol 2009;46:474–81.
[12] Priori SG, Chen SR. Inherited dysfunction of sarcoplasmic reticulum Ca^{2+} handling and arrhythmogenesis. Circ Res 2011;108:871–83.
[13] Bers DM. Cardiac sarcoplasmic reticulum calcium leak: basis and roles in cardiac dysfunction. Annu Rev Physiol 2014;76:107–27.
[14] Chen W, Wang R, Chen B, Zhong X, Kong H, Bai Y, et al. The ryanodine receptor store-sensing gate controls Ca^{2+} waves and Ca^{2+}-triggered arrhythmias. Nat Med 2014;20:184–92.
[15] Marx SO, Reiken S, Hisamatsu Y, Jayaraman T, Burkhoff D, Rosemblit N, et al. PKA phosphorylation dissociates FKBP12.6 from the calcium release channel (ryanodine receptor): defective regulation in failing hearts. Cell 2000;101:365–76.
[16] Li Y, Kranias EG, Mignery GA, Bers DM. Protein kinase A phosphorylation of the ryanodine receptor does not affect calcium sparks in mouse ventricular myocytes. Circ Res 2002;90:309–16.
[17] Guo T, Zhang T, Mestril R, Bers DM. Ca^{2+}/Calmodulin-dependent protein kinase II phosphorylation of ryanodine receptor does affect calcium sparks in mouse ventricular myocytes. Circ Res 2006;99:398–406.
[18] Gyorke I, Hester N, Jones LR, Gyorke S. The role of calsequestrin, triadin, and junctin in conferring cardiac ryanodine receptor responsiveness to luminal calcium. Biophys J 2004;86:2121–8.
[19] Knollmann BC, Chopra N, Hlaing T, Akin B, Yang T, Ettensohn K, et al. Casq2 deletion causes sarcoplasmic reticulum volume increase, premature Ca^{2+} release, and catecholaminergic polymorphic ventricular tachycardia. J Clin Invest 2006;116:2510–20.
[20] Chu G, Luo W, Slack JP, Tilgmann C, Sweet WE, Spindler M, et al. Compensatory mechanisms associated with the hyperdynamic function of phospholamban-deficient mouse hearts. Circ Res 1996;79:1064–76.
[21] Sipido KR, Vangheluwe P. Targeting sarcoplasmic reticulum Ca^{2+} uptake to improve heart failure: hit or miss. Circ Res 2010;106:230–3.
[22] Lakatta EG, Maltsev VA, Vinogradova TM. A coupled SYSTEM of intracellular Ca^{2+} clocks and surface membrane voltage clocks controls the timekeeping mechanism of the heart's pacemaker. Circ Res 2010;106:659–73.
[23] Kapoor N, Liang W, Marban E, Cho HC. Direct conversion of quiescent cardiomyocytes to pacemaker cells by expression of Tbx18. Nat Biotechnol 2013;31:54–62.
[24] Sirenko S, Maltsev VA, Maltseva LA, Yang D, Lukyanenko Y, Vinogradova TM, et al. Sarcoplasmic reticulum Ca^{2+} cycling protein phosphorylation in a physiologic Ca^{2+} milieu unleashes a high-power, rhythmic Ca^{2+} clock in ventricular myocytes: relevance to arrhythmias and bio-pacemaker design. J Mol Cell Cardiol 2014;66:106–15.
[25] Bai Y, Jones PP, Guo J, Zhong X, Clark RB, Zhou Q, et al. Phospholamban knockout breaks arrhythmogenic Ca^{2+} waves and suppresses catecholaminergic polymorphic ventricular tachycardia in mice. Circ Res 2013;113:517–26.
[26] Chen Z, Akin BL, Jones LR. Mechanism of reversal of phospholamban inhibition of the cardiac Ca^{2+}-ATPase by protein kinase A and by anti-phospholamban monoclonal antibody 2D12. J Biol Chem 2007;282:20968–76.
[27] Nivala M, Ko CY, Nivala M, Weiss JN, Qu Z. Criticality in intracellular calcium signaling in cardiac myocytes. Biophys J 2012;102:2433–42.
[28] Nivala M, Ko CY, Nivala M, Weiss JN, Qu Z. The emergence of subcellular pacemaker sites for calcium waves and oscillations. J Physiol 2013;591:5305–20.
[29] Picht E, Zima AV, Blatter LA, Bers DM. SparkMaster: automated calcium spark analysis with ImageJ. Am J Physiol 2007;293:C1073–81.
[30] Restrepo JG, Weiss JN, Karma A. Calsequestrin-mediated mechanism for cellular calcium transient alternans. Biophys J 2008;95:3767–89.
[31] Nivala M, de Lange E, Rovetti R, Qu Z. Computational modeling and numerical methods for spatiotemporal calcium cycling in ventricular myocytes. Front Physiol 2012;3:114.
[32] Wegener AD, Simmerman HK, Lindemann JP, Jones LR. Phospholamban phosphorylation in intact ventricles. Phosphorylation of serine 16 and threonine 17 in response to beta-adrenergic stimulation. J Biol Chem 1989;264:11468–74.
[33] Akin BL, Jones LR. Characterizing phospholamban to sarco(endo)plasmic reticulum Ca^{2+}-ATPase 2a (SERCA2a) protein binding interactions in human cardiac sarcoplasmic reticulum vesicles using chemical cross-linking. J Biol Chem 2012;287:7582–93.
[34] Lukyanenko V, Gyorke S. Ca^{2+} sparks and Ca^{2+} waves in saponin-permeabilized rat ventricular myocytes. J Physiol 1999;521(Pt 3):575–85.
[35] Lukyanenko V. Permeabilization of cell membrane for delivery of nano-objects to cellular sub-domains. Methods Mol Biol 2013;991:57–63.
[36] Jamur MC, Oliver C. Permeabilization of cell membranes. Methods Mol Biol 2010;588:63–6.
[37] Keller M, Kao JP, Egger M, Niggli E. Calcium waves driven by "sensitization" wavefronts. Cardiovasc Res 2007;74:39–45.
[38] Hoit BD, Khoury SF, Kranias EG, Ball N, Walsh RA. In vivo echocardiographic detection of enhanced left ventricular function in gene-targeted mice with phospholamban deficiency. Circ Res 1995;77:632–7.
[39] DeSantiago J, Maier LS, Bers DM. Frequency-dependent acceleration of relaxation in the heart depends on CaMKII, but not phospholamban. J Mol Cell Cardiol 2002;34:975–84.
[40] Huser J, Bers DM, Blatter LA. Subcellular properties of $[Ca^{2+}]_i$ transients in phospholamban-deficient mouse ventricular cells. Am J Physiol 1998;274:H1800–11.
[41] Vangheluwe P, Tjwa M, Van Den Bergh A, Louch WE, Beullens M, Dode L, et al. A SERCA2 pump with an increased Ca^{2+} affinity can lead to severe cardiac hypertrophy, stress intolerance and reduced life span. J Mol Cell Cardiol 2006;41:308–17.
[42] Louch WE, Vangheluwe P, Bito V, Raeymaekers L, Wuytack F, Sipido KR. Phospholamban ablation in hearts expressing the high affinity SERCA2b isoform normalizes global Ca^{2+} homeostasis but not Ca^{2+}-dependent hypertrophic signaling. Am J Physiol Heart Circ Physiol 2012;302:H2574–82.